SAR Observation of Ionosphere Using Range/Azimuth Sub-bands

Jun Su, Kim, DLR, Microwaves and Radar Institute, junsu.kim@dlr.de, Germany
Konstantinos, Papathanassiou, DLR, Microwaves and Radar Institute, kostas.papathanassiou@dlr.de, Germany

Abstract

In SAR applications, the ionosphere is normally considered as a disturbance that has to be removed or compensated for. In this paper the ionosphere is the objective of observation. This is motivated by the fact that nowadays polarimetric SAR systems can provide high resolution ionospheric maps that are not possible using conventional ionospheric mapping tools. This paper investigates a set of new ionospheric parameters that can be observed and mapped by SAR by exploring range and azimuth sub-bands. The range sub-bands are used to estimate the ionosphere independently of polarimetry. The azimuth sub-bands are related to the three-dimensional geometry of the ionosphere, as well as, to its dynamic component. The potential to estimate these parameters from SAR sub-bands is discussed and first results using ALOS PALSAR data are presented.

1 Introduction

The disturbing effects of ionosphere on SAR images have been studied for decades. The primary goal was/is to predict and to correct the ionospheric distortions on SAR focusing, interferometry and polarimetry. These studies, however, show gradually clear that the accurate knowledge of the spatial distribution of ionosphere is the key for a successful correction [1], [2]. Interestingly, this knowledge can be provided by the SAR data itself. Indeed, quad-pol SAR data can map the lateral distribution of the ionosphere in terms of Total Electron Content (TEC) with an unprecedented high resolution [1], [3] exploiting the Faraday rotation induced by it.

Besides the estimation of Faraday rotation, which performs best at full-band in order to increase the number of looks available, sub-bands SAR images are expected to be able to provide more information about the ionosphere. As the ionosphere is a dispersive media, range sub-bands experience different level of dispersion. The studies in [4] and [5] have shown that such effect can be used for the estimation of (differential) TEC. The azimuth sub-bands are related to the squint induced parallax. This turns into the ability of resolving the vertical structure of the ionosphere as mentioned in [6] and validated in [7]. At the same time, the azimuth sub-bands has a reduced synthetic aperture, and can be therefore used to reduce the effect of the scintillation [8] at the cost of spatial resolution.

This paper proposes the use of range and azimuth sub-bands for the retrieval of ionospheric parameters. First of all the ability to estimate absolute TEC using range sub-bands, hence independently of polarisation, is discussed. Secondly, the vertical structure of electron density and the (possible) drift velocity of the ionosphere are retrieved using azimuth sub-bands.

Case	f_0 (GHz)	W (MHz)	ϕ_{quad} (°)
TSX	9.65	150	0.12
ALOS PALSAR	1.27	28	1.85
ALOS-II	1.27	85	17.1
BIOMASS	0.435	6	0.53

Table 1: Quadratic phases in (2) of some past and future SAR missions for 20 TECU. Centre frequency $\boldsymbol{f_0}$, range bandwidth $\boldsymbol{W}$, and quadratic phase $\boldsymbol{\phi_{quad}}$.

2 Single-pol TEC Estimation

Due to the dispersive nature of the ionosphere each frequency component of the chirp signal experiences a different phase advance. For a two-way propagation the ionospheric phase advance is [1]

$$\phi = -\frac{4\pi\zeta}{cf}TEC, \tag{1}$$

where $\zeta = \frac{q_e^2}{8\pi^2\epsilon_0 m} \approx 40.31$ m^3/s^2, q_e and m are the charge and the mass of electron, ϵ_0 the vacuum permittivity, c the speed of light, and f the frequency of the signal. In a relatively narrow bandwidth around the centre frequency f_0, ϕ can be linearly expanded as

$$\phi(\Delta f) \approx \frac{-4\pi\zeta TEC}{cf_0}\left(1 - \left(\frac{\Delta f}{f_0}\right) + 2\left(\frac{\Delta f}{f_0}\right)^2\right). \tag{2}$$

Among the three TEC-proportional terms in (2), the quadratic term is further considered because only the dispersion in the ionosphere can induce the quadratic phase with respect to frequency. In a band-limited chirp signal of bandwidth W ($-\frac{W}{2} < \Delta f < \frac{W}{2}$), however, the contribution of the quadratic term is small. **Table 1** shows the quadratic phases calculated for past and future SAR systems when TEC =20 TECU. The largest quadratic phases are expected for ALOS or ALOS-II, but even there they are small. Therefore, the estimation of the quadratic phase is explored theoretically.

The quadratic phase component of a coherent scatterer in the k-th range sub-band image out of N non-overlapping equally divided sub-band images is

$$\phi_k = \phi_0 + \beta\left(\frac{kW}{N}\right)^2 + \epsilon_k, \tag{3}$$

where k is an integer between $-\frac{N-1}{2}$ and $\frac{N-1}{2}$, ϵ_k is the noise phase term in the k-th range sub-band image, and $\beta = -8\pi\zeta TEC/cf_0^3$ is the quadratic phase coefficient in the frequency domain. β can be estimated from (3) with an accuracy given by

$$\sigma_\beta^2 = \frac{90}{W^4 SCR}, \tag{4}$$

where SCR is signal to clutter ratio of the coherent scatterer. This result is identical to the accuracy of Doppler rate estimation in auto-focusing implementations [9]. Combination of (2) and (4) yields the TEC estimation accuracy from L coherent scatterers

$$\sigma_{TEC} = \frac{3\sqrt{10}cf_0^3}{8\pi\zeta W^2\sqrt{SCR}\sqrt{L}}. \tag{5}$$

From (5), it is clear that the estimation of TEC with the standard deviation of TECU level is possible in the ALOS PALSAR single-pol's 28 MHz bandwidth with 10^5 number of coherent scatterers of 20dB of SCR. We thanks to Francesco De Zan for this analysis.

3 Azimuth Sub-bands

3.1 Ionosphere Tomography

In each azimuth sub-band, the ground is imaged at different squint angles. Any combination of two different azimuth sub-bands would introduce a parallax that can be used to measure the distance to the scatterer. **Figure 1** shows a simple case in which an ionospheric thin-layer is imaged by two azimuth sub-bands, one approaching (blue) and the other departing (red). The ionosphere is placed between the ground and the sensor. In the approaching sub-band, the ionosphere is imaged forward, and in the departing sub-band, it is imaged backward. The spatial separation of the ionospheric features on two different sub-band images in the azimuth direction (L_{sep}) is proportional to the height of the ionospheric layer (h_{iono}) because of the similarity of triangles. Therefore, h_{iono} can be estimated as [7]

$$h_{\text{iono}} = 2R\cos\theta \cdot \frac{L_{\text{sep}}}{L_{\text{SA}}}, \tag{6}$$

where R is the zero-Doppler distance, θ is the look-angle, and L_{SA} is the synthetic aperture length.

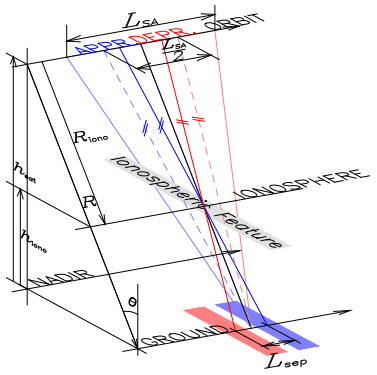

Figure 1: Imaging geometry of the ionospheric feature between ground and sensor using two sub-bands.

An example of ionospheric altitude estimation using two azimuth sub-bands is shown in **Figure 2**. Shown ALOS PALSAR data is acquired on April 1st 2007 near Fairbanks, Alaska through an active ionosphere. The top panel shows the estimated Faraday rotation, and the bottom one shows the profiles of Faraday rotation at approaching (blue) and departing (red) sub-bands along the range lines marked with the black rectangle. The observed L_{sep} is 3 km. Given L_{SA} of ALOS PALSAR around 20 km, $\theta = 24^\circ$, and $R = 800$ km, h_{iono} is found to be 220 km from (6). The estimated value fits well with ground measurements by a nearby station HAARP [10].

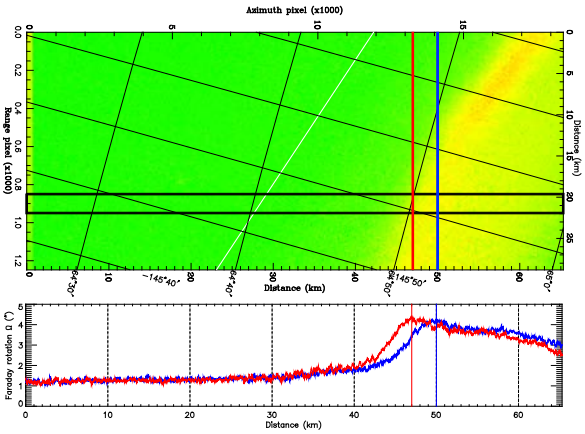

Figure 2: Estimation of Faraday rotation (top panel) and the azimuth sub-band profiles (bottom panel). The red profile corresponds to departing sub-band and the blue profile to approaching one.

The azimuth spectrum can be divided more than two sub-bands. With a larger number of narrower azimuth sub-bands, a three dimensional reconstruction of the ionosphere is possible. This reconstruction is carried out in the plane defined by the slant range direction and the orbit. Next, the orbit-slant range plane is meshed into

the resolution cells in which the tomogram will be calculated. Each ionospheric distortion (observation) is caused by the electron density of the individual mesh grids in the line of sight. Meshing the plane coarse enough, the number of observations of ionospheric feature is sufficient to over-determine the linear problem.

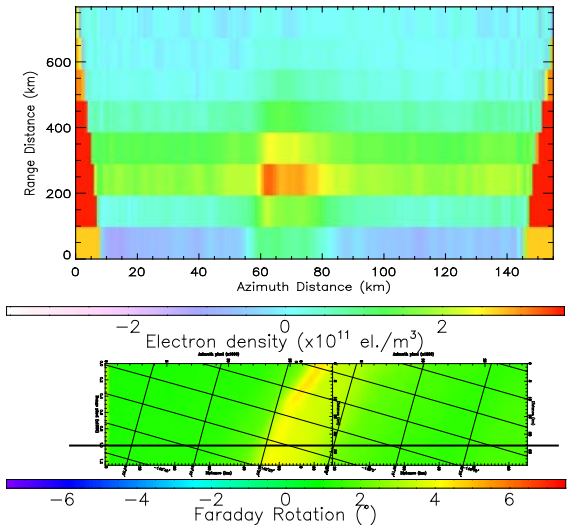

Figure 3: Example of ionospheric tomogram using Faraday rotations of azimuth sub-bands. The tomogram (top) corresponds to the range marked by black line on the Faraday rotation map at bottom.

An example of such a tomogram obtained using the Faraday rotation estimates of two sequential ALOS PALSAR acquisitions in azimuth is shown in **Figure 3**. The left acquisition of bottom figure is the same data shown in **Figure 2**. The orbit-slant range plane is meshed using rectangular grids of range direction resolution of $R_0/8$ (approximately 100 km), the azimuth direction resolution of 1 km. Red colour indicates a high electron content in that resolution cell; blue colour indicates a lower concentration. The effect of ray-bending is not considered. A Chapman layer with its peak at 250 km with scale height of 100 km is *a priori* assumed. The retrieved tomogram is strongly dependent on the selection of *a priori* information due to the ill-conditioned observation geometry.

An important drawback of such tomographic approaches is that they are applicable only when the ionosphere has significant spatial variation in the azimuth direction. For correcting SAR data, however, this constraint does not cause problems because a constant or smooth ionosphere does not cause significant image distortions.

3.2 Drift Velocity Field

Under different geometric conditions of orbit and geomagnetic field along which the ionospheric features are aligned, the interpretation of azimuth sub-band analysis is different. At equator, differently from the polar regions, the orbit and the geomagnetic fields are quite parallel. Thus, the ionospheric features do not move forward or backward (different from **Figure 1**), and the parallax between different azimuth sub-bands does not give significant variation to map the vertical structure of the electron density distribution.

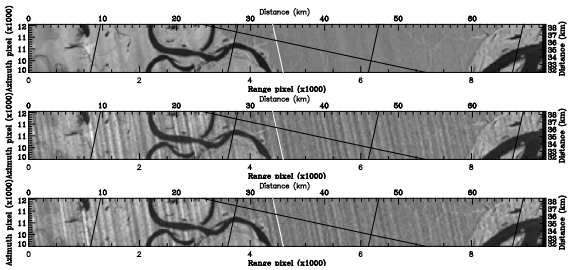

Figure 4: Full azimuth band image (top), and 1/16 bandwidth in approaching (middle) and departing (bottom) azimuth sub-bands acquired over the north-west part of Brazil. The white line at the middle is the projected direction of the geomagnetic field on a 400 km altitude level.

SAR images acquired over equatorial regions at the local evening times often shows amplitude stripes aligned nearly parallel to the geomagnetic field [11]. The pattern of the stripes becomes more visible when it is imaged using only a part of azimuth bandwidth as shown in **Figure 4**. This is because the integration effect of the narrower sub-band is lower than the full azimuth bandwidth. Comparing the two sub-band images of different squint angles, the ionospheric features (in this case, the amplitude stripes) are displaced in the range direction.

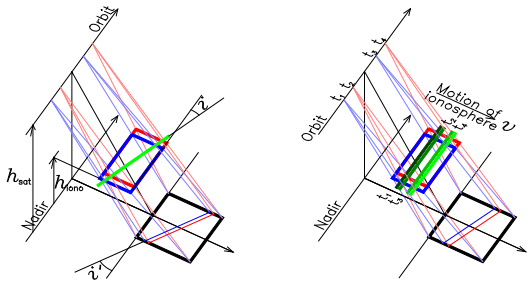

Figure 5: Interpretation of moving amplitude stripes with in azimuth sub-bands. Left: The imaging geometry component. Right: The dynamic component.

There are two effects that may interpret the moving amplitude stripes in the azimuth sub-looks: The first one is the imaging geometry (left panel of **Figure 5**). Let the angle between the orbit and the amplitude stripe is i. As

the squint angle changes, the amplitude stripes are imaged gradually at the further range. For negative i, they are imaged nearer. This prediction coincides with **Figure 4**, where i is negative, and the amplitude stripes are shifted to the nearer range.

However, the geometric interpretation cannot explain the inhomogeneity of the amplitude stripes displacement. The second effect can be the drift of the ionosphere itself (right panel of **Figure 5**). The altitudes of the ionosphere (h_{iono}) and the satellite (h_{sat}), the angle between amplitude stripes and the orbit on the ground projected SAR image i', the observed displacement x and the drift velocity v are related as

$$x = L_{\mathrm{SA}} \cdot \tan i' \cdot \frac{h_{\mathrm{iono}}}{h_{\mathrm{sat}}} + \frac{h_{\mathrm{sat}} \cdot v}{h_{\mathrm{sat}} - h_{\mathrm{iono}}} \Delta t, \qquad (7)$$

where Δt is the duration of aperture synthesis. The drift velocity field can be, therefore, immediately derived from the displacement field estimated from the azimuth sub-band images and an ionospheric altitude (which is unknown).

However, there are several possible error sources in the estimation of the ionospheric drift velocity field. Firstly the relation between the amplitude stripes on SAR image and the ionospheric electron density distribution might not be related so straight forwardly. That means the interpretation requires more complex models than simple geometries. Secondly the vertical structure of the ionosphere can be more complex than the thin-layer assumption, presenting also spatial variation.

4 Conclusion

This paper proposes several approaches of using range and azimuth sub-bands to estimate ionospheric parameters. The application of range sub-bands in the detection of absolute TEC independently of polarisation was discussed. ALOS-II that will start operation in 2014 with up to 85 MHz bandwidth is expected to provide the first reliable TEC estimates aside from Faraday rotation measurements. Azimuth sub-bands can be applied in more diverse ways limited to the case of ionosphere with large variations. At polar regions, where the (polar) orbit and the geomagnetic field are nearly orthogonal, the parallax of sub-bands could be used to resolve the vertical structure of the ionosphere. The ionospheric altitudes can be estimated and the vertical structure of electron densities can be profiled. Along the equator, azimuth sub-bands can resolve small-scale amplitude stripes, as well as, can provide the possibility of measuring drift velocity field maps. Comparisons with reference measurements are required to validate the proposed methodology and to assess its performances.

References

[1] F. J. Meyer and J. B. Nicoll, "Prediction, Detection, and Correction of Faraday Rotation in Full-Polarimetric L-band SAR Data," *IEEE Transactions on Geoscience and Remote Sensing*, vol. 46, no. 10, pp. 3076-3086, October 2008.

[2] J. S. Kim, K. P. Papathanassiou, S. Quegan and N. Rogers, "Estimation and correction of scintillation effects on spaceborne P-band SAR images," in *IGARSS 2012*, Munich, Germany, 2012.

[3] X. Pi, A. Freeman, B. Chapman, P. Rosen and Z. Li, "Imaging ionospheric inhomogeneities using spaceborne synthetic aperture radar," *Journal of Geophysical Research*, vol. 116, no. A04303, pp. 1-13, April 2011.

[4] R. Brcic, A. Parizzi, M. Eineder, R. Bamler and F. Meyer, "Ionospheric effects in SAR interferometry: an analysis and comparison of methods for their estimation," in *IGARSS*, Vancouver, 2011.

[5] P. A. Rosen, S. Hensley, F. Meyer and T. Ainsworth, "Further developments in ionospheric mitigation of repeat-pass InSAR data," in *IGARSS*, Honolulu, 2010.

[6] U. Wegmüler, C. Werner, T. Strozzi and A. Wiesmann, "Ionospheric electron concentration effects on SAR and INSAR," in *Proc. IGARSS2006*, Denver, USA, 2006.

[7] J. S. Kim, Development of Ionosphere Estimation Techniques for the Correction of SAR Data, Zürich: Ph.D. Disseration, Swiss Federal Institute of Technology, 2013.

[8] S. Quegan, J. J. Green and J. Chen, "Simultation of ionospheric disturbances and impact assessment on BIOMASS product quality," Sheffield, 2009.

[9] J. F. Green and C. J. Oliver, "The limit on autofocusing in SAR," *Internaltional Journal of Remote Sensing*, vol. 13, no. 14, pp. 2623-2641, 1992.

[10] "The High Frequency Active Aurora Research Program," [Online]. Available: http://www.haarp.alaska.edu/cgi-bin/digisonde/ionogram.cgi?request=1175412601&dir=next. [Accessed 17 October 2011].

[11] M. Shimada, Y. Muraki and Y. Otsuka, "Discovery of anoumoulous stripes over the Amazon by the PALSAR onboard ALOS satellite," in *IGARSS2008*, Boston, USA, 2008.